ISSN1027-5495. Functional Materials, 32, No.1 (2025), p. 115-125
doi:http://dx.doi.org/10.15407/fm32.01.115 © 2025 — STC "Institute for Single Crystals"

Majorana and Dirac fermion excitations in $La_{0.15}Sm_{0.85}MnO_{3+\delta}$, controlled by external magnetic field

F.N. Bukhanko

Donetsk Institute for Physics and Engineering named after. O.O. Galkin
NASU, 46 Nauky ave., Kyiv, 03028, Ukraine

Received August 19, 2024

The possibility of excitation of Majorana and massless Dirac fermions in self-doped manganites controlled by an external magnetic field is established. It is shown that in the ZFC mode of magnetization measurement, the excitation of Majorana fermions dominates, while in the FC mode the main contribution to the "supermagnetization" of the sample is made by the excitation of Dirac fermions. During remagnetization of $La_{0.15}Sm_{0.85}MnO_{3+\delta}$ manganites at 4.2 K, the single and double cone-shaped features of $M(H)$ were found near $H = 0$ in the magnetization reversal isotherms. These peculiarities of magnetization demonstrate the evolution of the Dirac fermions magnetic excitations at quantum phase transitions in the 2D Dirac semimetal, induced by the merging and splitting of two Dirac points. The evolution of thermal excitation of two Majorana zero modes in the first and second Landau band with an increase in the strength of the external magnetic field was also studied. An alternating permutation of the spiky double peaks and truncated hill features of the magnetization $M(T)$ in $La_{0.15}Sm_{0.85}MnO_{3+\delta}$ may be explained by the existence of two well-known in the literature hidden states CSL1 and CSL2 of the chiral quantum spin liquid in this material.

Keywords: 2D Dirac semimetal, Dirac and Majorana fermions, topological phase transitions, single and double cones-like features magnetization, Majorana zero modes

Ферміонні збудження Майорани та Дірака в $La_{0.15}Sm_{0.85}MnO_{3+\delta}$, керовані зовнішнім магнітним полем. *Ф.М. Буханько*

Встановлено можливість збудження майоранівських і безмасових ферміонів Дірака в самолегованих манганітах, керованих зовнішнім магнітним полем. Показано, що в ZFC-режимі вимірювання намагніченості домінує збудження майоранівських ферміонів, а в FC-режимі основний внесок у «надмагніченість» зразка вносить збудження дираківських ферміонів. Під час перемагнічування манганітів $La_{0.15}Sm_{0.85}MnO_{3+\delta}$ при 4,2 К були знайдені одинарні та подвійні конусоподібні особливості $M(H)$ поблизу $H = 0$ на ізотермах перемагнічення. Ці особливості намагніченості демонструють еволюцію магнітних збуджень дираківських ферміонів при квантових фазових переходах у двовимірному дираківському напівметалі, викликаних злиттям і розщепленням двох дираківських точок. Досліджено також еволюцію теплового збудження двох майоранівських нульових мод у першій і другій зони Ландау зі збільшенням напруженості зовнішнього магнітного поля. Поперемінна перестановка гострих подвійних піків і усічених горбистих особливостей намагніченості $M(T)$ в $La_{0.15}Sm_{0.85}MnO_{3+\delta}$ може бути пояснена існуванням у цьому матеріалі двох добре відомих у літературі прихованих станів CSL1 та CSL2 хіральної квантової спинової рідини.

1. Introduction

In work [1], the theoretically predicted and experimentally confirmed topological nodal lines of semimetals were considered, with special attention paid to the mechanisms of protecting the symmetry of nodal lines in various materials. Three different protection mecha-

nisms are discussed: a combination of inversion and time-reversal symmetry, mirror reflection symmetry, and non-symmorphic symmetry, and their robustness under the effect of spin orbit coupling (SOC). It was shown that Dirac semimetal (DSM) is the result of two doubly degenerate bands crossing near the Fermi level at a discrete point in k-space, known as the Dirac point. Demanded by both inversion and time-reversal symmetry, the four-fold degenerate Dirac point has a band dispersion that is linearly dependent on k. Such a linearly dispersed band structure causes the low energy excitations near the crossing point being Dirac fermions. At the same time, the Weyl semimetal (WSM) state arises when either inversion symmetry or time reversal symmetry is broken. Doubly degenerate bands become spin split when considering the SOC, separating into two singly degenerate band crossings called Weyl points. The existence of Weyl points near the E_F leads to several special characteristics including Fermi arcs on the surface. In contrast to DSMs and WSMs, which have zero dimensional band crossings**,** Dirac nodal-line semimetals (NLSs) have extended band crossings along special lines in k-space. Research on graphene has triggered a tremendous interest in the physics of two-dimensional (2D) Dirac fermions in condensed-matter physics [2]. In undoped graphene, the valence band touches the conduction band at the Fermi level isotropically in a linear manner. The structure of the low-energy band, as well as the form of the underlying Hamiltonian, resembles the structure of massless fermions, commonly studied in high-energy physics, with two significant differences. First, graphene electrons are constrained to move in two spatial dimensions, whereas within the framework of relativistic quantum mechanics it was established that fermions can be described in three spatial dimensions. And second, in condensed-matter physics, the characteristic velocity is not the speed of light but the Fermi velocity, which is approximately two orders of magnitude less than the former. In addition to graphene, Dirac fermions have now been discovered in various other systems in condensed matter physics, for example on the surfaces of three-dimensional topological insulators or in quasi-two-dimensional organic materials, or in specially designed systems ("artificial graphenes"), such as e.g. cold atoms in optical lattices, molecular crystals or microwave crystals. The low-energy electronic properties of graphene can be obtained with high accuracy within a simplified tight-binding model, where only hopping between nearest-neighboring p_z orbitals is taken into account, with a characteristic energy scale of $t \approx 3$ eV. The simplified tight-binding model takes into account hopping between nearest-neighboring sites, e.g. from A to B_1, B_2 and B_3. In the case of undistorted graphene, the associated three hopping amplitudes are identical due to the point symmetry of the lattice. The fact that the Dirac points coincide with the corners of the Brillouin zone in the case of graphene is a consequence of the crystal point symmetry. The undistorted graphene lattice provides isotropic Dirac points, $\boldsymbol{v_1} = (v_F, 0)$ and $\boldsymbol{v_2} = (0, v_F)$, and Hamiltonian becomes $H^{\xi}_{\boldsymbol{q}} = v_F (\xi q_x \sigma^x + q_y \sigma^y)$. This Hamiltonian exactly corresponds to the Hamiltonian of massless Dirac fermions of relativistic quantum mechanics in two spatial dimensions. The energy spectrum of the so-called Landau levels can be obtained directly with the help of the eigenstates of the numerical operator and exhibits the characteristic $\sqrt{Bn}$ scaling observed in magneto-spectroscopic measurements and scanning-tunneling spectroscopy. Thus, at zero energy, the dynamical properties of the A sublattice are completely separated from the dynamic properties of sublattice B. This leads to the emergence of a special series of quantum Hall effects at filling factors $\nu = n_{el} / n_B = \pm 2(2n + 1)$, where n_{el} is the 2D electronic density and $n_B = 1/2\pi l^2_B = eB / h$ is the the flux density of quanta penetrating the graphene sheet. The effect manifests itself by plateaus in the transverse (Hall) resistance, at magnetic fields corresponding to these filling factors, accompanied by zeros in the longitudinal resistance. The observation of quantum Hall's states at filling factors was interpreted as direct evidence for the presence of pseudo-relativistic carriers in graphene, described in terms of massless Dirac fermions. Dirac points appear as topological objects characterized by a charge. This charge describes the wave function in reciprocal space when turning around the Dirac point. A pair of such Dirac points with opposite charge related by time-reversal symmetry can move in reciprocal space or even be annihilated. In the case of lattice with the square symmetry, the Brillouin zone is a square. The Dirac points are now located inside the first Brillouin zone (BZ). Moreover, upon variation of the band parameters, the two Dirac points may approach each other and merge into a single point D_0. The lo-

cation of this merging point is simply $\boldsymbol{D}_0 = \boldsymbol{G} / 2$, where $\boldsymbol{G}$ is a reciprocal lattice vector. The condition for the existence of Dirac points defines a manifold in the space of band parameters. This manifold separates a semimetallic phase with two Dirac cones from a band insulator. The merging of the Dirac points in D_0 marks the transition between a semi-metallic phase and an insulating phase. It can be analyzed topologically in terms of winding numbers – below the transition, the semi-metallic phase is characterized by two Dirac points of opposite charge that are annihilated at the transition. The resulting zero topological charge then allows for the opening of a gap in the spectrum and a transition to an insulating phase. In order to describe the transition more quantitatively, authors introduce the gap parameter Δ_* , which changes its sign at the transition. When Δ_* is negative, the spectrum exhibits the two Dirac cones at a distance $2\,q_D = 2\sqrt{-2m^*\Delta_*}$ and a saddle point in $\boldsymbol{D}_0$ (the energy of the saddle point being $\pm\,|\Delta_*|$). With increasing Δ_* from negative to positive values, the saddle point shifts to lower energies and eventually disappears into the hybrid semi-Dirac point at the transition ($\Delta_* = 0$), before a gap of size $2\Delta_* > 0$ occurs in the spectrum. Therefore, the Hamiltonian can also be viewed as interpolation between the behaviors of isolated Dirac points, such as in graphene, and massive particles in the gap phase. In particular, the Landau level spectrum in a magnetic field continuously evolves from the well-known $\sqrt{nB}$ spectrum as in graphene to the spectrum of massive particles $(n + 1/2)B$ above the merging transition. While below the transition at sufficiently low magnetic fields, there are closed orbits encircling only one of the Dirac points (with a winding number $|w_i| = 1$), and therefore, a doubly degenerate zero-energy level is obtained; above the transition, the situation is drastically different. Indeed, all possible orbits then have a winding number $w = 0$ that yields the 1/2 offset in the Landau-level spectrum, as in the case of conventional Schrödinger fermions. Directly at the transition, the level spectrum shows an unusual behavior $[(n + 1/2)\mathrm{B}]^{2/3}$. Again the 1/2 offset is due to the absence of closed orbits encircling singular points with $w \neq 0$ at the transition. Notice, however, that the topological transition in the presence of a magnetic field is not abrupt. Below the transition, where the zero-field spectrum exhibits two Dirac points, the two Dirac points are coupled by the magnetic field. In this case, the closed orbits necessarily enclose surfaces of size $1/l^{\,2}_B \propto B$ in reciprocal space, due to the non-commutativity of the kinetic-moment operators. At sufficiently large magnetic fields, Dirac points separated by small wave vectors are no longer resolved. This removes the original two-fold degeneracy of the zero-energy level $n = 0$ in an exponential manner. These quantum phase transitions are accompanied by a violation of the mirror, inversion and time-reversal symmetry upon sign reversal external magnetic field, typical for the Dirac topological semimetals. In this work, excitation of Majorana and Dirac fermions was first studied in two hidden topological states of chiral quantum spin liquid in $La_{0.15}Sm_{0.85}MnO_{3+\delta}$.

2. Material and methods

Samples of self-doped manganites $La_{0.15}Sm_{0.85}MnO_{3+\delta}$ ($\delta \sim 0.1$) were obtained from high-purity oxides of lanthanum, samarium and electrolytic manganese, taken in a stoichiometric ratio. The synthesized powder was pressed under pressure 10 kbar into discs with a diameter of 6 mm, a thickness of 1.2 mm and sintered in air at a temperature of 1170 ºC for 20 h, followed by cooling at a rate of 70◦C/h. According to X-ray structural analysis, the obtained tablets were single-phase ceramics. X-ray studies were carried out at 300K on a DRON-1.5 diffractometer in Ni-$K_{\alpha 1+\alpha 2}$ radiation. The symmetry and crystal lattice parameters were determined by the positions and characteristic splitting of the reflections of the pseudocubic lattice of the perovskite type. Temperature and field dependences of DC magnetization were measured using a VSM EGG (Princeton Applied Research) vibrating magnetometer and a nonindustrial magnetometer in ZFC and FC modes. When measuring the temperature dependences of the magnetization $M(T)$ in the ZFC mode, the sample was first cooled to 4.2 K in a zero external magnetic field, followed by an increase in temperature to the required value. In the FC mode for measuring the magnetization $M(T)$, the sample was first cooled to 4.2 K in magnetic fields of various strengths, followed by heating. The field dependences of the magnetization $M(H)$ were measured during sample remagnetization at a temperature of 4.2 K in a wide range of magnetic fields in the ZFC and FC measurement modes.

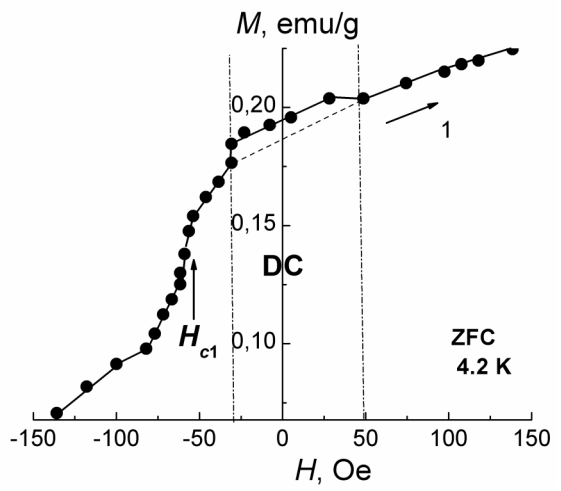

Fig. 1. Fragment of magnetization isotherm 1 of the field dependence $M(H)$ in $La_{0.15}Sm_{0.85}MnO_{3+\delta}$ at 4.2 K in the ZFC measurement mode in the range of magnetic fields ±150 Oe.

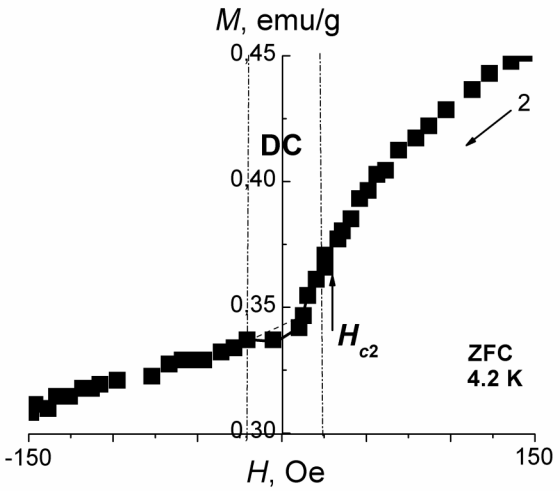

Fig. 2. Fragment of demagnetization isotherm 2 of the field dependence $M(H)$ in $La_{0.15}Sm_{0.85}MnO_{3+\delta}$ at 4.2 K in the ZFC measurement mode in the range of magnetic fields ±150 Oe.

3. Results and discussion

In the processes of magnetization reversal of $La_{0.15}Sm_{0.85}MnO_{3+\delta}$ at 4.2 K in the ZFC and FC measurement modes, the sample magnetization $M(H)$ grows linearly with increasing magnetic field strength in a wide range of ± 5 kOe, which is typical for paramagnets and antiferromagnets. As can be seen from Fig.1 and 2, the DC magnetization has pronounced unusual threshold features near zero fields. The supermagnetization is caused by the excitation of fermions near zero magnetic field during magnetization reversal of the sample. The strong field hysteresis is also unusual, the width of which in the FC measurement mode is much larger than in the ZFC mode. As can be seen from Fig. 1, 2, in the process of magnetization reversal in the ZFC mode near the critical fields $H_{c1} \approx$ -50 Oe and $H_{c2} \approx$ 50 Oe, threshold features are formed, respectively, for the magnetization isotherm – 1 and demagnetization – 2. The hump-like asymmetric feature of the M (H) plots is formed in the range of magnetic fields of ± 500 Oe with increasing magnetic field strength in the positive direction. This unusual feature is a superposition of a relatively narrow threshold feature of magnetization near the critical field $H_{c1} \approx$ -50 Oe, which is superimposed on a smooth drop in the supermagnetization to zero near magnetic fields of ± 500 Oe in the form of a tail. The dominant contribution to the growth of supermagnetization in isotherm 1 with increasing field is made by a clearly pronounced positive jump in magnetization near the field $H_{c1} \neq 0$. This feature is characteristic of the low-energy excitation of a wide 2D continuum of Majorana fermions during the phase transition of a chiral QSL to a state with a topological order, which was considered earlier in [3–18]. However, according to Figs. 1 and 2, there are also additional contributions ± ΔM to the magnetization M (H) in the form of cone-shaped features located in a narrow range of magnetic fields near the zero. These additional new features are shaped like a hill with a cut-off top.

According to [1, 2], such features are direct evidence of the excitation of massless 2D Dirac fermions in quasi-two-dimensional spin systems. Thus, the observation of the single and double cone-shaped features of magnetization near zero field can be explained by the presence of pseudo-relativistic carriers in $La_{0.15}Sm_{0.85}MnO_{3+\delta}$ described in terms of Dirac fermions. The M (H) plots obtained in the magnetic field range of ±500 Oe in the ZFC mode with increasing magnetic field strength in the positive direction (isotherm 1) demonstrate an asymmetric feature consisting of two contributions that differ in shape and intensity: an asymmetric hump-shaped feature in the field range of ±500 Oe and a narrower single cone-shaped positive contribution +ΔM near H = 0. A similar complex feature of the M (H) plots is also observed with a decrease in the field during reversal cycle on isotherm 2 (Fig. 2). In Fig. 2 it is clearly seen that during sample demagnetization near zero field, the magnetic response of the spin system has the form of a threshold drop in supermagnetization with decreasing

field near the critical value $H_{c2} \approx 50$ Oe and additional very weak negative cone-shaped contribution $-\Delta M$ near $H = 0$. The critical fields, shape and intensity of the threshold low-energy excitation of quasiparticles in relation to the total magnetization differ significantly on the two isotherms, that is, a strong hysteresis is observed in the magnetization-demagnetization processes of the sample. It should also be noted that there is an unusual asymmetry of the M (H) curves for the left ($H < 0$) and right ($H > 0$) halves of the field dependences of the quantum spin liquid magnetization in isotherms 1 and 2, which can be explained by the violation of the mirror symmetry of the sample magnetization upon reversal of the sign of the external magnetic field. Thus, according to the field dependences of the magnetization in the ZFC measurement mode at a temperature of 4.2 K, with an increase in the strength of the external magnetic field, a second-order threshold quantum phase transition of the QSL to the state with topological order occurred, which is accompanied by a threshold excitation of Majorana fermions. As a result of this transition, in the magnetization reversal isotherms 1 and 2, near $H = 0$, intensive hump-like features of the magnetization are formed, the shape and intensity of which depend significantly on the direction of the growth of the magnetic field.

There are also weak additional contributions of Dirac fermions $\pm \Delta M$ to the magnetization M (H) in the form of cone-shaped features located in a narrow range of fields near the zero magnetic field, which are in good agreement with the literature data for 2D Dirac materials [1, 2, 19 - 24]. Therefore, we have for the first time achieved the simultaneous excitation of quasi-two-dimensional Majorana and massless Dirac fermions in a quantum spin liquid in a weak external magnetic field. Of great interest are also the magnetization reversal isotherms 1, 2 obtained in the FC measurement mode, from which it can be seen how single and double cone-shaped features of M (H) are formed during the magnetization reversal of the sample near the zero magnetic field. These features dominate in isotherms 1 and 2. This indicates that measurements of the magnetization field dependences in the FC mode are more favorable for studying the dynamics of Dirac cone-shaped excitations in a magnetic field. These features of supermagnetization arising when the direction of the vector $\boldsymbol{H}$ is inverted, are superimposed on a smooth drop in magnetization to zero with increasing field strength near magnetic fields of ± 500 Oe. In the FC mode of measuring magnetization, with increasing H (isotherm 1), near $H = 0$, a very narrow positive jump in magnetization ΔM is observed in the form of a single cone-shaped feature of the M (H) curves. More clearly, the formation of a new additional feature of supermagnetization near zero magnetic field manifested itself in the form of a wide double cone-shaped drop $-\Delta M$ near $H = 0$ in isotherm 2 during the demagnetization of the sample. Thus, in the processes of magnetization reversal of $La_{0.15}Sm_{0.85}MnO_{3+\delta}$ at 4.2 K in the ZFC and FC measurement modes, in the range of weak magnetic fields 100-200 Oe near the zero field, a non-dispersive ultranarrow zone of excited states Z_2 chiral QSL is formed, similar to flat bands in topological superconductors. The field dependences of the magnetization $M(H)$ obtained in this work for $La_{0.15}Sm_{0.85}MnO_{3+\delta}$ in the ZFC mode at a temperature of 4.2 K indicate that with an increase in the strength of the external magnetic field, a second-order threshold quantum phase transition of the QSL to the state with topological order occurs, followed by a smooth transition to the polarized phase. As a result of this transition, hump-shaped features of magnetization $M(H)$ are formed on the magnetization reversal isotherms of samples 1 and 2 near the value $H = 0$, the shape and intensity of which depend significantly on the direction of growth of the magnetic field. These features are typical for the low-energy excitation of a wide 2D continuum of Majorana fermions during the phase transition of a chiral QSL to a state with a topological order, which was considered earlier in [3–18]. An important consequence of the Kitaev model [3] is the splitting of electrons into a set of unusual quasiparticles, Majorana fermions; the splitting leads to the appearance of several Majorana fermion bands in the spectrum of magnetic low-energy excitations of the ground state of chiral spin liquids; the width of these bands depends significantly on magnetic gauge fluxes and external perturbations.

More recently, evidence of this splitting was found in α-$RuCl_3$ using the neutron scattering method, which was explained in [11]. In [11], a theoretical study of the dynamic structure factor $S^{ab}(\mathbf{q}, \omega)$ of a two-dimensional quantum spin liquid in gapless and gap phases was carried out in the framework of the Kitaev model for a hexagonal spin lattice. The existence of unusual hump-like features of the structure

factor caused by the excitation of the continuum of Majorana fermions and the appearance of gauge fluxes was shown. It was found that both in the gap and gapless phases of the QSL, the response vanishes at excitation energies below the gap Δ, which is directly related to the appearance of the gauge field. For excitation energies higher than the gap energy Δ, nonzero fermion contributions to the structure factor $S^{ab}(\omega)$ arise only from excited states with a parity opposite to that of the ground state. As a result, two modes of excitation of Majorana fermions are realized – Mode I and Mode II. Mode II contains a spiky response, while Mode I has no spiky response. In case I, the ground state of the QSL has an odd number of excitations, while in case II, magnetic excitations are either absent or their number is even. In Mode I, a broad hump-like magnetic response to external excitation is observed, while in Mode II, the response should be narrow. The responses may overlap or be separate. For case I, the response, broad in energy ω, is dominated by single-particle excitations; therefore, it manifests itself only within the width of the band of material fermions. In [13], exact results were obtained for the structure factor in the gap and gapless, Abelian and non-Abelian phases of the QSL. The structure factor has features in the appearance of quasiparticles in the form of Majorana fermions and fluxes Z_2 of the gauge field. In addition to a broad hump-like continuum of fractional spin excitations, the authors found spiky features in the magnetic response. These spiky features arise either from excited states containing only static magnetic fluxes and no mobile fermions, or from excited states in which fermions are closely coupled to fluxes. The structural factor is significantly different in the Abelian and non-Abelian QSLs. Coupled fermion-flow composites appear only in the non-Abelian phase. The main feature of the dynamical structure factor at the isotropic point of the non-Abelian phase ($J_x = J_y = J_z$) is the presence of a pointed δ-component caused by Majorana fermions coupled to flow pairs and a broad bump-like component caused by fermion continuum excitation. The beginning of the broad feature of the magnetic response corresponds to the edge of the Majorana fermion band. It should be noted that the width of the response of free fermions practically coincides with the width of the calculated function of the density of states $N(\omega)$ of Majorana fermions in the zero-flux phase. As noted in [13], different representatives of the family of Kitaev Hamiltonians correspond to a set of qualitatively different responses. What all these reactions have in common is that the found spin correlations are ultrashort: the structure factor contains the contributions from correlators of only local or nearest neighbors that have the same spin components. This is a consequence of the static nature of the resulting Z_2 gauge flows. Therefore, only the dependences of the dynamic structure factor S ($q = 0$, ω) on the excitation frequency were presented in the work. In all cases, the dynamic response has a gap, regardless of the existence of a gap in the excitation spectrum of the quantum spin liquid. The minimum gap Δ corresponds to the case of the formation of pairs of flows in the QCL in adjacent cells of the crystal lattice. The plot of one of the broad components of the magnetic response S ($q = 0$, ω) corresponds to the excitation of Majorana fermions. Its low-energy beginning corresponds to the gap Δ in the phase with gapless Majorana excitations, while the end is in the gap Majorana phase. As shown in the paper, this broad response arises when one or two fermions are excited, depending on the spin component and the parameters of the Hamiltonian. In the case of $J_x/J_z = J_y/J_z$, there are only two response components $S^{zz}(\omega)$ and $S^{xx}(\omega) = S^{yy}(\omega)$. For the Abelian states of the QSL, it was found that in the isotropic model the response $S^{\alpha\alpha}$ (ω) is not equal to zero at excitation energies higher than the energy Δ required to create pairs of flows. This dominant contribution comes from single excitations of Majorana fermions, but the tail is pulled to higher energies. To provide explanation for the rarity of 2D Dirac materials to find clues for searching for new Dirac systems, the authors [19] reviewed the recent theoretical aspects of various 2D Dirac materials, including graphene, silicene (silicone), germanene, graphynes, several boron and carbon sheets, transition metal oxides and artificial lattices (electron gases and ultracold atoms). It was shown that Dirac cones are quite stable to perturbations. For example, when a uniaxial or shear strain is applied, the band structure of graphene keeps gapless and the Dirac point moves to a new k location near the original one. At present, Dirac cone merging is achieved only in artificial honeycomb lattices where parameters are much more adjustable. By patterning CO molecules on clean Cu(111), the hexagonal potential lattice of electron gases was effectively modulated to demonstrate a transition from

massless to massive Dirac fermions in the system. In an ultracold gas of 40 K atoms trapped in a 2D honeycomb lattice of optical potential, the merging and annihilation of two Dirac points were clearly recorded when the lattice anisotropy exceeds a critical limit. A simplified analysis on a general 2D system, which contains two atoms of the same species in each unit cell, demonstrated that a hexagonal cell is the most favorable for the existence of Dirac cones, and the favorableness is gradually diminished when the cell evolves into a square one. According to [19], to obtain Dirac materials, at least three conditions are required: (1) Symmetry. Specific symmetries are required to reduce the number of equations to be solved. The *k*-points should be unchanged after the symmetry operation (invariant *k*-point). Too low or too high symmetries are both disadvantageous. (2) Parameters. Even when the number of equations is equal to the number of variables, the solution does not necessarily exist since the variables (k_x and k_y) are real numbers and appear in the equations in the form of a sine or cosine function. Therefore, proper parameters are required. This is usually described as a phase diagram in the parameter space. (3) Fermi level and band overlap. The Fermi level must lie at the Dirac points, and there must be no bands other than the Dirac points overlapping at the Fermi level. In [20], an ultracold Fermi gas of atoms at 40 K in a two-dimensional tunable optical lattice was investigated, which can be continuously adjusted to create square, triangular, dimer and honeycomb structures. The momentum resolution of interband transitions was used to directly observe the motion of Dirac points. Starting from a honeycomb lattice the authors gradually increased the tunneling along the *x* direction by decreasing the intensity of the X beam. The positions of the Dirac points continuously approached the corners of the Brillouin zone, as expected from an *ab initio* calculation of the two-dimensional band structure. When reaching the corners, the two Dirac points merge, annihilating each other. There the dispersion relation becomes quadratic along the q_y axis, remaining linear along q_x. Beyond this critical point, a finite band gap appears for all quasi-momenta of the Brillouin zone. This situation signals a transition between band structures of two different topologies, one of which contains two Dirac points and the other none. In [21] it was shown, that introducing lattice anisotropy leads to a displacement of the Dirac cones in response to the applied strain, leaving a pseudogap at the original Dirac points. Here, a group-theory analysis is combined with first-principles calculations to reveal the movement characteristics of Dirac points and band gaps in various graphynes under rotational uniaxial and shear strains. Graphene, where linear effects dominate, is different from α-, ß- and γ-graphynes which generate strong nonlinear responses due to their bendable acetylenic linkages. However, the linear components of the electronic response, which are essential in determining material performance such as intrinsic carrier mobility due to electron–phonon coupling, can be readily separated, and are well described by a unified theory. The movement of the Dirac points in α-graphyne is circular under a rotational strain, and the pseudogap opening is isotropic with a magnitude of only 2% that in graphene.

According to [22], there has been a recent growing interest for various physical systems exhibiting a multiband excitation spectrum with crossing points between the bands. This interest was boosted by the discovery of graphene, where the low energy spectrum is described by a 2D Dirac equation for massless fermions, giving the name "Dirac point" to such linear crossing point. In two dimensions, the band touching is a topological defect protected by time-reversal and inversion symmetries. This contact point is characterized by a winding number *w* which describes the winding of the phase of the wave function when moving around this point in reciprocal space. Such singularities may emerge or disappear when changing external parameters, provided that the sum of their winding numbers is conserved. In [23] the authors proposed a simple Hamiltonian H_{eff} to describe the motion and merging of Dirac points in the electronic spectrum of two-dimensional electrons. This merging is a topological transition which separates a semimetallic phase with two Dirac cones from an insulating phase with a gap. They calculated the density of states and the specific heat. The spectrum in a magnetic field *B* is related to the resolution of the Schrödinger equation in a double well potential. The spectrum in the vicinity of the topological transition is very well described by a semiclassical quantization rule. This model describes continuously the coupling between valleys associated with the two Dirac points, when approaching the transition. It reproduces the low-field part of the Rammal

Hofstadter spectrum for a honeycomb array remarkably well.

In [24], the electronic properties of a deformed honeycomb structure formed by semiconductor quantum dots (QDs) were analyzed theoretically using the tight binding method. By applying the compressive or tensile deformation of the honeycomb lattice, the variation of energy spectrum has been explored. It was shown that, the massless Dirac fermions are generated in this adjustable system and the positions of the Dirac cones as well as the slope of the linear dispersions could be manipulated. Furthermore, a clear linear correspondence between the distance of movement d (the distance from the Dirac points to the Brillouin zone corners) and the tunable bond angle a of the lattice are found in this artificial planar QD structure. These results provide the theoretical basis for manipulating Dirac fermions and should be very helpful for the fabrication and application of high-mobility semiconductor QD devices. The fact that doped manganites can have the properties of a 2D semimetal has been known for a long time, but relatively little theoretical and experimental work has been done in this interesting area of solid state physics. The possibility of the existence of a state similar to an exciton dielectric in doped $La_{1-x}Ca_xMnO_3$ manganites was first pointed out in [25] within the framework of a two-band model of double exchange of charge carriers in the e_g shell of manganese ions without taking into account the electron–phonon interaction. It was shown that in the initial $LaMnO_3$ compound, there is a nesting of electron and hole regions (pockets) of the Fermi surface, corresponding to two e_g bands of charge carriers. As a result of the nesting of these bands in $LaMnO_3$, charge carriers are unstable to the formation of a gas of electron-hole pairs of the exciton dielectric type. A small dielectric gap appears in the spectrum of quasiparticles, and the system becomes an insulator. The anomalies in the temperature dependences of the *ac*-dielectric permittivity found in the $La_{1-y}Sm_yMnO_{3+\delta}$ system were explained in [26] in terms of the existing concepts of the Bose–Einstein condensation of an electron–hole liquid in the form of metal drops in an exciton dielectric. In our later work [27], when explaining the effect of external influences on the magnetism of fluctuating low-dimensional electron and spin correlations in frustrated manganites $La_{1-y}Sm_yMnO_{3+\delta}$ (y = 0.85,1.0) we considered several weak coupling models of the appearance of CDW/SDW states and superconductivity, based on the possibility of the existence of an unusual state − an exciton condensate − in some materials, in which new types of charge/spin density and superconductivity waves can arise under the influence of weak external influences.

According to [28], in a typical one-dimensional (1D) multi-fermion system, an arbitrarily weak short-range repulsive interaction completely destroys the Fermi liquid, thereby giving rise to so-called Luttinger behavior. In higher dimensions (2D and 3D), the Fermi liquid is considered more robust, although it is not expected to remain absolutely stable. While in the case of short-range repulsive interactions, any deviations from the Fermi liquid are likely to be limited to the regime of infinitely strong couplings, the long-ranged interactions are considered to be generally capable of destroying the Fermi liquid even at finite couplings. In the case of Fermi liquids with screened repulsive interactions, the same scenario describes the excitonic instability. It should be noted, however, that the transition driven by a variable density (which provides a more appropriate picture of the system, in which the number of carriers is not fixed) can still be a second-order transition. In that regard, the class of systems with isolated ("nodal") Fermi points, in which the density of states of quasiparticles (DOS) vanishes, appears to be particularly promising. As a result, any long-ranged interaction (whether the bare Coulomb one or that mediated by soft collective modes propagating near an emergent instability) remains largely unscreened. Examples of the nodal fermion systems are provided by degenerate semimetals, such as graphite or bismuth, where the conduction and valence bands touch each other at isolated points in the Brillouin zone. In a monolayer of graphite, for example, the two-dimensional fermion excitations with the momenta close to the nodal points have a linear dispersion, and, therefore, can be described in terms of a Dirac-like effective theory [29 - 31].

Previously the formation of a broad continuum of spinon pair excitations in $SmMnO_{3+\delta}$ in the "weak magnetic field" regime H = 100 Oe, 1 kOe in the FC mode was explained in the framework of the Landau quantization models of the compressible spinon gas with fractional values of the factor v filling three overlapping bands with quantum numbers n = 1, 2, and 3. In the regime of "strong magnetic field"

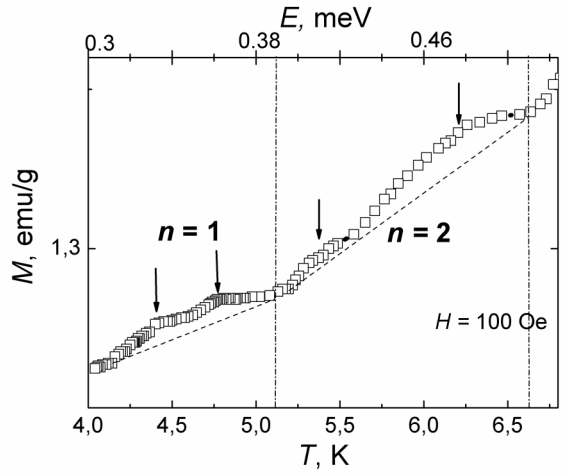

Fig. 3. The thermal excitation of two coupled Majorana zero modes in Landau zones n = 1, 2 in interval temperatures 4.2 – 7 K in the external magnetic field H = 100 Oe.

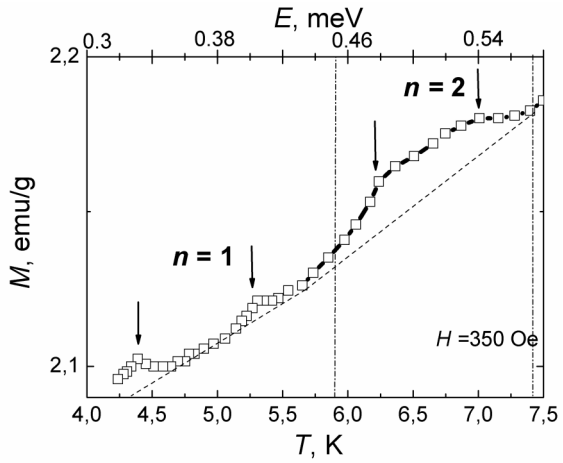

Fig. 4. The thermal excitation of two coupled Majorana zero modes in Landau zones n = 1, 2 in interval temperatures 4.2 – 7.5 K in the external magnetic field H = 350 Oe.

H =3.5 kOe, the new step-like quantum oscillations of temperature dependences of supermagnetization of incompressible spinon liquid were found [32]. In this work, the thermal excitation of two coupled Majorana zero modes with energy $E_{\mathrm{MZM}} \cong 0.35$ meV in the form of two wide overlapping peak features on the temperature dependence of the magnetization has been detected in the first Landau zone with n = 1 of the quantized spectrum of fermions in $La_{0.15}Sm_{0.85}MnO_{3+\delta}$ in external magnetic field H = 100 Oe (Fig. 3). As can be clearly seen from the figure, the temperature dependence of the supermagnetization of the sample M (T) in the first Landau zone in the magnetic field 100 Oe has the shape of a truncated hill with a flat top near the average temperature $T_{\mathrm{MZM}} \cong$ 4.6 K. According to [1, 2], the observation of quantum Hall states at the fractional filling factors may be interpreted as direct evidence for of the presence of pseudo-relativistic carriers in $La_{0.15}Sm_{0.85}MnO_{3+\delta}$, described in terms of massless 2D Dirac fermions, which corresponds to the excitation of two coupled Majorana zero modes arising on point defects [33–43]. A slight increase in the magnetic field up to 350 Oe led to a dramatic change in the shape of the temperature dependence of magnetization in the Landau zone with n = 1: a singularity of supermagnetizatiom M(T) in a field H = 350 Oe has a distinct shape of two weak spiky peaks near the average temperature $T \cong$ 5 K (Fig.4). According to [11, 13, 16], these spiky features in the magnetic response arise from excited states containing either only static magnetic fluxes and no mobile fermions, or from excited states in which fermions are closely coupled to fluxes. The structural factor is significantly different in the Abelian and non-Abelian QSLs. Coupled fermion-flow composites appear only in the non-Abelian phase. The main feature of the dynamical structure factor at the isotropic point of the non-Abelian phase is the presence of a pointed δ-component caused by Majorana fermions coupled to flow pairs and a broad hump-like component caused by fermion continuum excitation. In external magnetic field H = 1 kOe, magnetic response appears in the first Landau zone in the shape of a truncated hill with a flat top near the average temperature $T_{\mathrm{MZM}} \cong$ 4.6 K, which corresponds to the excitation of two coupled Majorana zero modes arising on point defects (Fig. 5). An alternating permutation of the spiky double peaks and truncated hill features of the magnetization M(T) with increasing strength H of the external magnetic field were also discovered in the second Landau zone (Fig. 2-5). The alternating permutation of the spiky double peaks and truncated hill features of the magnetization M(T) in $La_{0.15}Sm_{0.85}MnO_{3+\delta}$ may be explained by the existence of two well-known hidden states of the chiral spin liquid in this material [33]. In external magnetic field H = 3.5 kOe, only the step-like quantum oscillations of temperature dependences of supermagnetization of incompressible quantum spinon liquid were found. The so-called Majorana bound states arising on point defects [33–42] have attracted great interest. They can be interpreted as own antiparticles in the sense that, in the language of second quantization, the operators of creation

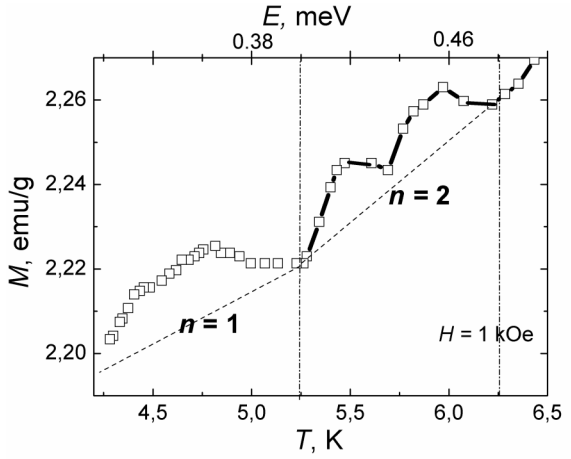

Fig. 5. The thermal excitation of two coupled Majorana zero modes in Landau zones $n = 1, 2$ in interval temperatures 4.2 – 7.5 K in the external magnetic field $H = 1$ kOe.

and annihilation of bound states are equal to each other. This means that Majorana bound states carry both zero spin and zero charge. Majorana bound states arise exactly at zero energy and are separated from other ordinary quasiparticle excitations by a finite energy gap. For this reason, Majorana bound states are also often referred to as Majorana zero modes (MZM). It has been shown that MZMs in a 2D material obey quantum exchange statistics, which are neither fermionic nor bosonic [34–40]. MZMs are supposed to be an example of so-called non-Abelian anyons. This means that the replacement of two MZMs implements a non-trivial rotation of the degenerate subspace of the ground state, while subsequent rotations do not necessarily commute. This property makes non-Abelian anyons such as MZM promising potential building blocks for topological quantum computers, where logic gates would then be performed by exchanging anions [41, 42]. However, not all anyons are useful in topological quantum computing. Only non-Abelian anyons are useful. The simplest realization of a non-Abelian anyon is a quasiparticle or a defect that maintains Majorana's zero mode. The zero mode refers to zero-energy mid-band excitations to which these localized quasi-particles typically correspond in a low-dimensional topological superconductor. This is a real fermionic operator commuting with the Hamiltonian. The existence of such operators guarantees the topological degeneracy of the system. The term "Majorana" refers to the fact that these fermionic operators are real, just as the Majorana version of the Dirac equation is real. However, the key concept here is the non-Abelian anyon, and MZMs are a special mechanism by which non-Abelian anyons, commonly referred to as Ising anyons, can be generated. The simplest experimental result confirming the existence of MZM states is a zero-shift tunneling conductivity peak in a semiconductor (InSb or InAs) nanowire in contact with a conventional metallic superconductor (Al or Nb), which appears only when a finite external magnetic field is applied to the wire. Anyons can appear in two ways: as localized excitations or as defects in an ordered system. Fractionally charged excitations of Laughlin's quantum Hall fluid are an example of the former. An example of the latter is the Abrikosov vortices in a topological superconductor.

4. Conclusions

According to the experimental results presented in this paper, we first have carried out the simultaneous excitation of quasi-two-dimensional Majorana and massless Dirac fermions in a quantum spin liquid in a weak external magnetic field in the form of well known hump–like and cones-like features located in a narrow range of fields near the zero magnetic field. These results indicate the existence of a close relationship between the Majorana and Dirac fermions in $La_{0.15}Sm_{0.85}MnO_{3+\delta}$, which allows a better understanding of the results of our previous works. These additional new features are shaped like a hill with a cut-off top. According to literature data, the similar features are direct evidence of the excitation of massless 2D Dirac fermions in quasi-two-dimensional spin systems. Thus, the observation of the single and double cone-shaped features of magnetization near zero field can be explained by the presence of pseudo-relativistic carriers in $La_{0.15}Sm_{0.85}MnO_{3+\delta}$ described in terms of Dirac fermions.

References

1. S.-Y. Yang, H. Yang, E. Derunova et al., *Advances in Physics*, *X,*1 (2017).
2. M. Goerbig G.Montambaux, *Matière de Dirac, S´eminaire Poincar´e,* **XVIII**: 23 (2014).
3. A. Kitaev, *Annals of Physics,* **321**, 2 (2006).
4. H. Yao, S.A. Kivelson, *Phys.Rev. Lett.*, **99**, 247203 (2007).
5. H.C. Jiang, Z.C. Gu, X.L. Qi et al., *Phys. Rev.* B, **83**, 245104 (2011).
6. S. Trebst, P. Werner, M. Troyer et al., *Phys.Rev. Lett.*, **98,** 070602 (2007).

7. J. Vidal, S. Dusuel, K.P. Schmidt, , *Phys. Rev. B*, **79**, 033109 (2009).
8. I.S., Tupitsyn, A. Kitaev, N.V. Prokof'ev et al, *Phys. Rev. B*, **82**, 085114 (2010).
9. S. Dusuel, M. Kamfor, R. Orus et al., P*hys. Rev. Lett.*, **106,** 107203 (2011).
10. E. Fradkin, S.H. Shenker, *Phys. Rev. D,* **19**, 3682 (1979).
11. J. Knolle, D.L. Kovrizhin, J.T. Chalker et al., *Phys. Rev. Lett.*, **112**, 207203 (2014).
12. K.S. Tikhonov, M.V. Feigelman, *Phys. Rev. Lett.*, **105**, 067207 (2010).
13. J. Knolle, D.L. Kovrizhin, J.T. Chalker et al., *Phys. Rev.* B, **92**, 115127 (2015).
14. V. Lahtinen, *New J. Phys.*, **13**, 075009 (2011).
15. G. Baskaran, S. Mandal, R. Shankar, *Phys. Rev. Lett.*, **98**, 247201 (2007)
16. J. Knolle, R. Moessner, *Annu. Rev. Condens. Matter Phys.***10**, 451 (2019).
17. T. Senthil, A. Vishwanath, L. Balents et al., *Science,* **303**, 1490 (2004).
18. A.W. Sandvik, *Phys. Rev. Lett.,* **98**, 227202 (2007).
19. J. Wang, S. Deng, Z. Liu et al., *Natl. Sci. Rev*, **2** (1), 22 (2015).
20. L.Tarruell, D. Greif, T. Uehlinger et al., arXiv:1111.5020v2 cond-mat.quant-gas. 25 Jun 2013, 1-6.
21. Z. Li, Z. Liu, Z. Liu, *Nano Research,* **10**(6), 2005 (2017).
22. G. Montambaux, L.-K. Lim, J.-N. Fuchs et al., *Phys. Rev. Lett.,* **121**, 256402 (2018).
23. G. Montambaux, F. Piéchon, J.-N. Fuchs et al., arXiv:0907.0500v1 cond-mat.mes-hall. 2 Jul 2009, 1 - 18.
24. J. Peng, P.J. Chen, Y. Duan et al., *AIP Advances,* **5**, 037132 (2015).
25. D.V. Efremov, D.I. Khomskii, *Phys. Rev. B*, **72**, 012402. (2005).
26. F.N. Bukhanko, A.F. Bukhanko, *Fiz.Tverd.Tela*, **57**, 1098 (2015).
27. F.N. Bukhanko, A.F. Bukhanko, *Fiz.Tverd.Tela*, **61,** 2493 (2019).
28. D.V. Khveshchenko, W.F. Shively, arXiv:cond-mat/0510519v3 cond-mat.str-el. 21 Apr 2006.
29. J. González, F. Guinea, M.A.H. Vozmediano, *Phys. Rev. Lett.*, **69**, 172 (1992).
30. J. González, F. Guinea, M.A.H. Vozmediano, *Phys. Rev. Lett*., **77**, 3589 (1996).
31. J. González, F. Guinea, M.A.H. Vozmediano, *Phys. Rev.* B, **63**, 134421 (2001).
32. F.N. Bukhanko , A.F. Bukhanko, *Fiz. Nizk. Temp*. **47**, 1021 (2021).
33. K. Laubscher, J. Klinovaja, arXiv:2104.14459v2 cond-mat.mes-hall. 13 Aug 2021.
34. G. Moore, N. *Read, Nucl. Phys.* B, **360,** 362 (1991).
35. G.E. Volovik, *JETP Lett.*, **70**, 609 (1999).
36. N. Read, D. Green, *Phys. Rev. B*, **61**, 10267 (2000).
37. T. Senthil, M.P.A. Fisher, *Phys. Rev. B,* **61**, 9690 (2000).
38. D.A. Ivanov, *Phys. Rev. Lett.*, **86**, 268 (2001).
39. G.E. VolovikThe Universe in a Helium Droplet (Oxford University Press, Oxford, 2003).
40. G.E. Volovik, *JETP Lett*. **90,** 398-401. (2009)
41. A.Y. Kitaev, *Ann. Phys.*, **303**, 2 (2009).
42. C. Nayak, S.H. Simon, A. Stern et al., *Rev.Mod. Phys.*, **80**, 1083 (2008).